

# A Fermionic bi-Doublet Effective Field Theory for Dark Matter

---

**D. Karamitros\***

*University of Ioannina, Greece*

*E-mail: [dkaramit@cc.uoi.gr](mailto:dkaramit@cc.uoi.gr)*

We study an effective field theory which includes the Standard Model extended by a Dark Sector consisting of two fermionic  $SU(2)_L$ -doublets. A  $Z_2$  parity guarantees that, after electroweak symmetry breaking, the lightest neutral particle is stable, acting as a WIMP. The dark sector interacts with the Higgs and gauge bosons through renormalizable and non-renormalizable  $d = 5$  operators. We find that a WIMP with a mass around the electroweak scale, *i.e.* accessible at the LHC, is consistent with collider and astrophysical data only when non-trivial magnetic dipole interactions with the gauge bosons exist.

*Corfu Summer Institute 2016 "School and Workshops on Elementary Particle Physics and Gravity"  
31 August - 23 September, 2016  
Corfu, Greece*

---

\*Speaker.

## 1. Introduction

There is a number of evidence suggesting that the mass content of the universe is dominated by Dark Matter (DM). From CMB measurements, the DM seems to account for about 25% of the total energy of the universe [1]. One of the most promising DM candidates is the so-called Weakly Interacting Massive Particle (WIMP). The WIMP is assumed to be a massive electrically neutral stable particle interacting weakly with the Standard Model (SM). Under these assumptions, the mass of the WIMP seems to lie naturally at the electroweak scale, due to the so-called *WIMP-miracle* [2]. This makes the WIMP accessible at LHC as well as direct detection experiments.

Here we present the work of [3], where the SM is extended by a pair of fermionic  $SU(2)_L$ -doublets, which constitutes the Dark Sector (DS). Assuming that the SM and the DS do not mix, due to a  $Z_2$  parity, the complete set of  $d = 5$  non-renormalizable operators is introduced. We show that after electroweak (EW) symmetry breaking there is a stable neutral particle, which can act as a WIMP. The EFT at hand generalises the discussion on the bi-doublet DM scenario. Among the models incorporating a pair of fermion doublets in their low-energy spectrum, one finds the *higgsino* DM case [4], some simplified models such as the doublet-triplet DM [5], non-supersymmetric  $SO(10)$  GUTs [6] and its left-right symmetric subgroup [7].

Performing a phenomenological analysis, we show that a viable WIMP with a mass close to the EW scale, i.e. suitable for LHC searches, acquires sizeable magnetic dipole moments with the gauge bosons.

## 2. The EFT content

In the SM we add a pair of fermion  $SU(2)_L$ -doublets,  $D_{1,2}$ , with opposite hypercharges,  $Y(D_1) = -Y(D_2) = -1$ . We impose a  $Z_2$  parity which separates the DS from the SM and ensures that the lightest neutral particle is stable and thus a WIMP candidate. Apart from the renormalizable interactions, we also introduce the complete set of  $d = 5$  non-renormalizable operators, which are responsible for the dipole interactions between the DS fermions and the SM gauge bosons, the Yukawa interactions and the mass splitting between the components of the doublets.

### 2.1 The Yukawa interactions

Since there are no renormalizable interactions between the Higgs boson and  $D_{1,2}$ , they appear at the  $d = 5$  level. The  $d = 5$  Yukawa along with the mass terms are<sup>1</sup>

$$\begin{aligned}
 -\mathcal{L}_{\text{mass+Yukawa}} \supset & \frac{y_1}{2\Lambda} (H^T \varepsilon D_1) (H^T \varepsilon D_1) + \frac{y_2}{2\Lambda} (H^\dagger D_2) (H^\dagger D_2) \\
 & + \frac{y_{12}}{\Lambda} (H^T \varepsilon D_1) (H^\dagger D_2) + \frac{\xi_{12}}{\Lambda} (D_1^T \varepsilon D_2) (H^\dagger H) + M_D D_1^T \varepsilon D_2 + \text{H.c.},
 \end{aligned} \tag{2.1}$$

where  $\Lambda$  is the cut-off of the EFT and  $\varepsilon$  is the  $SU(2)_L$  anti-symmetric tensor (in the fundamental representation). Also, for simplicity we assume that the parameters are real numbers, while the mass parameter  $M_D$  can be redefined to be positive. Finally, as it can be seen from eq.(2.1), there are four independent operators with their respective Wilson coefficients  $y_{1,2,12}$  and  $\xi_{12}$ .

<sup>1</sup>The spinor and gauge indices are suppressed for simplicity.

## 2.2 The dipole interactions

Apart from the operators of eq. 2.1, there are also interactions with the gauge bosons at  $d = 5$  level. These are

$$\begin{aligned} \mathcal{L}_{\text{dipoles}} \supset & \frac{d_Y}{\Lambda} D_1^T \sigma^{\mu\nu} \varepsilon D_2 B_{\mu\nu} + \frac{d_W}{\Lambda} (D_1^T \sigma^{\mu\nu} \varepsilon \vec{\tau} D_2) \cdot \vec{W}_{\mu\nu} + \\ & \frac{ie_Y}{\Lambda} D_1^T \sigma^{\mu\nu} \varepsilon D_2 \tilde{B}_{\mu\nu} + \frac{ie_W}{\Lambda} (D_1^T \sigma^{\mu\nu} \varepsilon \vec{\tau} D_2) \cdot \vec{\tilde{W}}_{\mu\nu} + \text{H.c.}, \end{aligned} \quad (2.2)$$

$B_{\mu\nu}$  ( $\vec{W}_{\mu\nu}$ ) the  $U(1)_Y$  ( $SU(2)_L$ ) gauge boson,  $d_Y$  and  $d_W$  are real numbers. Additionally, since we are not concerned about  $CP$  violation,  $e_Y = e_W = 0$ .

## 2.3 Symmetries of the Dark sector

### The custodial symmetry

It is known [8] that, the SM Higgs sector is invariant under a global  $SU(2)_R$  (custodial) symmetry. defining

$$\mathcal{H} = \begin{pmatrix} -H^{0*} & H^+ \\ H^- & H^0 \end{pmatrix}, \quad (2.3)$$

the SM Higgs sector is invariant under  $SU(2)_L \times SU(2)_R$  with the transformation rule  $\mathcal{H} \rightarrow U_L \mathcal{H} U_R$ . It turns out that in the EFT at hand the Yukawa sector exhibits the same symmetry, when

$$y_1 = y_2 = -y_{12}. \quad (2.4)$$

This can be seen by defining  $y \equiv -y_{12}$  and

$$\mathcal{D} = \begin{pmatrix} D_1^0 & D_2^+ \\ D_1^- & D_2^0 \end{pmatrix}, \quad (2.5)$$

which transforms as  $\mathcal{D} \rightarrow U_L \mathcal{D} U_R$ . Then the equation 2.1 obtains the form:

$$-\mathcal{L}_{Yuk} \supset \frac{y}{\Lambda} [\text{Tr}(\mathcal{H}^\dagger \mathcal{D})]^2 + M_D \det \mathcal{D} + \text{H.c.}, \quad (2.6)$$

which is clearly invariant under  $SU(2)_L \times SU(2)_R$ .

### The charge conjugation symmetry

In addition to the custodial symmetry, there is also a *charge conjugation* (c.c.) symmetry, which is a symmetry of the entire set of  $d = 5$  operators. For  $y_1 = y_2 = y$  (and  $\forall y_{12}$ ), the interactions 2.1 and 2.2 are invariant under exchanging  $D_1 \rightarrow D_2$  according to<sup>2</sup>

$$C^{-1} D_{2a} C = \varepsilon^{ba} D_{1b}. \quad (2.7)$$

This symmetry, basically, exchanges the columns of the matrix 2.5.

<sup>2</sup>In general the Higgs field is transformed as  $H \rightarrow H^\dagger$ , but in the Kibble parametrization  $H$  remains unaffected.

Finally, we should point out that in our phenomenological analysis we are going to study two *Benchmark* scenarios in the the c.c. symmetric limit i.e.  $y_1 = y_2$ . These two case are:

$$(a) y_{12} = -y, (b) y_{12} = 0. \quad (2.8)$$

The first one is the  $SU(2)_R$  symmetric limit, while the second violates the custodial symmetry, but is employed since it gives us a distinct mass spectrum.

### 3. The physical states

#### 3.1 Mass spectrum

After EW symmetry breaking, the Higgs field is shifted by its vacuum expectation value (vev),  $v$ , resulting to mixing between the components of  $D_{1,2}$ . After rotating to the mass basis, physical states are

$$\begin{aligned} \chi_1^0 &= \frac{1}{\sqrt{2}} (D_1^0 + D_2^0), & \chi_2^0 &= -\frac{i}{\sqrt{2}} (D_1^0 - D_2^0), \\ \chi^+ &= iD_2^+, & \chi^- &= iD_1^-. \end{aligned} \quad (3.1)$$

For these particles the mass terms become

$$\mathcal{L} \supset -m_{\chi^\pm} \chi^- \chi^+ - \frac{1}{2} \sum_{i=1}^2 m_{\chi_i^0} \chi_i^0 \chi_i^0 + H.c., \quad (3.2)$$

where the masses are

$$\begin{aligned} m_{\chi^\pm} &= M_D + \xi_{12} \omega, \\ m_{\chi_1^0} &= m_{\chi^\pm} + \omega (y - y_{12}), & \omega &\equiv \frac{v^2}{\Lambda}, \\ m_{\chi_2^0} &= m_{\chi^\pm} - \omega (y + y_{12}). \end{aligned} \quad (3.3)$$

As stated in the previous section, we consider the two *Benchmark* scenarios shown in 2.8. These produce two distinct hierarchies for the masses  $m_{\chi^\pm}, m_{\chi_{1,2}^0}$ .

The hierarchies are shown in Fig. 1. We note that for  $y < 0$  the lightest particle is always  $\chi_1^0$ , while for  $y > 0$ , the lightest particle becomes  $\chi_2^0$  without changing the phenomenology. Therefore, for the following analysis we are going to restrict  $y$  to be negative, which makes  $\chi_1^0$  our WIMP candidate. The masses of the particles for the two cases under study are:

**(a)**  $y = -y_{12} < 0$ . In this case, the heavy fermion is degenerate with the charged one, where the various masses are given by

$$m_{\chi_2^0} = m_{\chi^\pm}, m_{\chi_1^0} = m_{\chi^\pm} - 2\omega|y|.$$

**(b)**  $y < 0, y_{12} = 0$ . There is no degeneracy between the particles and the various masses are

$$m_{\chi_2^0} = m_{\chi^\pm} + 2\omega|y|, m_{\chi_1^0} = m_{\chi^\pm} - 2\omega|y|.$$

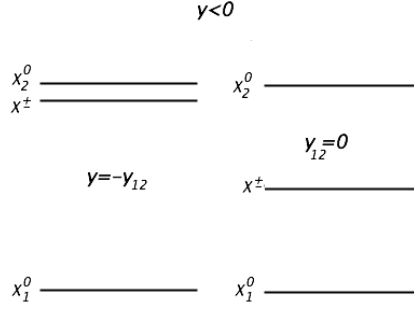


Figure 1: The mass hierarchies for the two Benchmark scenarios under study.

### 3.2 Interactions

We calculate the Yukawa interactions for the rotated fields. The Lagrangian describing the 3-point DS-Higgs interactions<sup>3</sup> is

$$\mathcal{L}_{\chi\chi h}^{\dim=5} \supset -Y^h \chi^- \chi^+ h \chi^- \chi^+ - \frac{1}{2} Y^h \chi_i^0 \chi_j^0 h \chi_i^0 \chi_j^0, \quad (3.4)$$

with

$$\begin{aligned} Y^h \chi^- \chi^+ &= \sqrt{2} \xi_{12} \frac{\omega}{v}, \\ Y^h \chi_1^0 \chi_1^0 &= \frac{\sqrt{2} \omega}{v} (\xi_{12} + y - y_{12}), \\ Y^h \chi_2^0 \chi_2^0 &= \frac{\sqrt{2} \omega}{v} (\xi_{12} - y - y_{12}), \\ Y^h \chi_1^0 \chi_2^0 &= 0. \end{aligned} \quad (3.5)$$

Interestingly, due to the c.c. symmetry, the interaction of the WIMP ( $\chi_1^0$ ) with the Higgs follows  $Y^h \chi_1^0 \chi_1^0 \sim \xi_{12} + y - y_{12}$ . Thus current Direct Detection experimental constraints (discussed later) can be avoided easily without the need for parameter fine tuning.

Since  $D_{1,2}$  are charged under  $SU(2)_L \times U(1)_Y$ , there are renormalizable interactions between them and the corresponding gauge bosons. The neutral ones are given by

$$\begin{aligned} \mathcal{L}_{neutral}^{\dim=4} \supset & -(+e) (\chi^+)^{\dagger} \bar{\sigma}^{\mu} \chi^+ A_{\mu} - (-e) (\chi^-)^{\dagger} \bar{\sigma}^{\mu} \chi^- A_{\mu} + \\ & \frac{g}{c_W} O'^L (\chi^+)^{\dagger} \bar{\sigma}^{\mu} \chi^+ Z_{\mu} - \frac{g}{c_W} O'^R (\chi^-)^{\dagger} \bar{\sigma}^{\mu} \chi^- Z_{\mu} + \\ & \frac{g}{c_W} O''^L_{ij} (\chi_i^0)^{\dagger} \bar{\sigma}^{\mu} \chi_j^0 Z_{\mu}, \end{aligned} \quad (3.6)$$

where

$$O'^L = O'^R = -\frac{1}{2}(1 - 2s_W^2) \text{ and } O''^L = -\frac{i}{2} \begin{pmatrix} 0 & 1 \\ -1 & 0 \end{pmatrix}, \quad (3.7)$$

<sup>3</sup>The 4-point interactions are not shown for simplicity.

with  $s_W = \sin\theta_W$  and  $\theta_W$  being the weak mixing angle. Notably, the interaction  $\chi_0^1 \chi_0^1 Z$  vanishes due to the charge conjugation symmetry.

Furthermore, the non-renormalizable operators of eq. 2.2 also contribute to the neutral interactions, where the 3-point ones are:

$$\begin{aligned} \mathcal{L}_{\text{neutral 3-point}}^{\text{dim}=5} \supset & -\frac{\omega}{v^2} (d_\gamma s_W + d_W c_W) O_{ij}^{\prime L} \chi_i^0 \sigma_{\mu\nu} \chi_j^0 F_Z^{\mu\nu} - \\ & \frac{\omega}{v^2} (d_\gamma s_W - d_W c_W) \chi^- \sigma_{\mu\nu} \chi^+ F_Z^{\mu\nu} + \\ & \frac{\omega}{v^2} (d_\gamma c_W - d_W s_W) O_{ij}^{\prime L} \chi_i^0 \sigma_{\mu\nu} \chi_j^0 F_\gamma^{\mu\nu} + \\ & \frac{\omega}{v^2} (d_\gamma c_W + d_W s_W) \chi^- \sigma_{\mu\nu} \chi^+ F_\gamma^{\mu\nu} + H.c., \end{aligned} \quad (3.8)$$

where  $F_\gamma$  and  $F_Z$  are the field strength tensors of the photon and  $Z$ , respectively. Interestingly, the dipole operators which arise at  $d = 5$  level, generate interactions between the neutral dark particles and the photon proportional to  $C_\gamma \equiv d_W s_W - d_\gamma c_W$ . There are also other interactions between  $W^\pm$  and the Dark Sector. The renormalizable ones are:

$$\begin{aligned} \mathcal{L}_{\text{charged 3-point}}^{\text{dim}=4} \supset & g O_i^L (\chi_i^0)^\dagger \bar{\sigma}^\mu \chi^+ W_\mu^- - g O_i^R (\chi^-)^\dagger \bar{\sigma}^\mu \chi_i^0 W_\mu^- + \\ & g O_i^{L*} (\chi^+)^\dagger \bar{\sigma}^\mu \chi_i^0 W_\mu^+ - g O_i^{R*} (\chi_i^0)^\dagger \bar{\sigma}^\mu \chi^- W_\mu^+, \end{aligned} \quad (3.9)$$

with

$$O_i^L = \frac{1}{2} \begin{pmatrix} i \\ -1 \end{pmatrix}, O_i^R = \frac{1}{2} \begin{pmatrix} i \\ -1 \end{pmatrix}. \quad (3.10)$$

From eq. 2.2, the 3-point interactions between  $W^\pm$  and the dark fermions become

$$\begin{aligned} \mathcal{L}_{\text{charged 3-point}}^{\text{dim}=5} \supset & -2\frac{\omega}{v^2} d_W O_i^{R*} \chi^- \sigma_{\mu\nu} \chi_i^0 F_{W^+}^{\mu\nu} + \\ & 2\frac{\omega}{v^2} d_W O_i^L \chi^+ \sigma_{\mu\nu} \chi_i^0 F_{W^-}^{\mu\nu} + H.c. \end{aligned} \quad (3.11)$$

Finally, we should point out that, due to an alignment of couplings in eqs. 3.6 and 3.9 with the those in eqs. 3.8 and 3.11, a ‘‘natural’’ cancellation of the  $d=4$  and  $d = 5$  contributions in the annihilation cross-section  $\chi_1^0 \chi_1^0 \rightarrow VV$  (with  $V$  being  $W$  and  $Z$ ) can be achieved. This, as we shall see later, will be important in obtaining the observed relic abundance for WIMP masses at the electroweak scale.

#### 4. ‘‘Earth constraints’’

In this section we study constraints, from WIMP( $\chi_1^0$ )-nucleon scattering experiments, searches for heavy charged fermions at LEP and from the LHC data for the Higgs boson decay to two photons. We collectively refer to these as ‘‘Earth constraints’’.

##### Nucleon-WIMP direct detection bounds

For the Spin-Independent cross-section the current limit set by the LUX Collaboration [9, 10] is  $\sigma_{\text{SI}} \sim \{1 - 3.5\} 10^{-45} \text{ cm}^2$ , for  $m_{\text{DM}} \sim \{100 - 500\} \text{ GeV}$ . This translates to

$$|Y^h \chi_1^0 \chi_1^0| \lesssim \{0.04, 0.06\}. \quad (4.1)$$

### LEP bounds

We next examine constrains for heavy charged fermions from LEP. From Fig. 1 we observe the next-to-lightest particle is the charged dark fermion,  $\chi^\pm$ , with mass  $m_{\chi^\pm} = M_D + \xi_{12} \omega$  that is assumed to be positive.

The bound on  $m_{\chi^\pm}$  from such experiments is [11]  $m_{\chi^\pm} \gtrsim 100$  GeV, which in terms of  $\xi_{12}$ ,  $\omega$  and  $M_D$  becomes  $\xi_{12} \gtrsim \frac{100 - M_D}{\omega}$ .

### Bound from $h \rightarrow \gamma\gamma$ measurements

From the interactions 2.1 and 3.8, the ratio  $R_{h \rightarrow \gamma\gamma} \equiv \frac{\Gamma(h \rightarrow \gamma\gamma)}{\Gamma(h \rightarrow \gamma\gamma)_{\text{SM}}}$  is given by [5]

$$R_{h \rightarrow \gamma\gamma} = \left| 1 + \frac{1}{A_{\text{SM}}} \frac{\sqrt{2} Y^h \chi^- \chi^+ \nu}{m_{\chi^\pm}} A_{1/2}(\tau) \right|^2, \quad (4.2)$$

where  $A_{\text{SM}} \simeq -6.5$  for  $m_h = 125$  GeV,  $\tau \equiv m_h^2/4m_{\chi^\pm}^2$  and  $A_{1/2}$  is the well known function given in Ref. [12]. The ratio  $R$  is currently under experimental scrutiny at LHC. The current value is  $R_{h \rightarrow \gamma\gamma} = 1.15_{-0.25}^{+0.28}$  [13]. From eq. 3.5 we expect that  $\xi_{12}$  would be restricted to small values from the loop induced  $h \rightarrow \gamma\gamma$  bound. This would also result to a lower bound on  $M_D$  at  $\sim 100$  GeV.

### Combined ‘‘Earth constraints’’

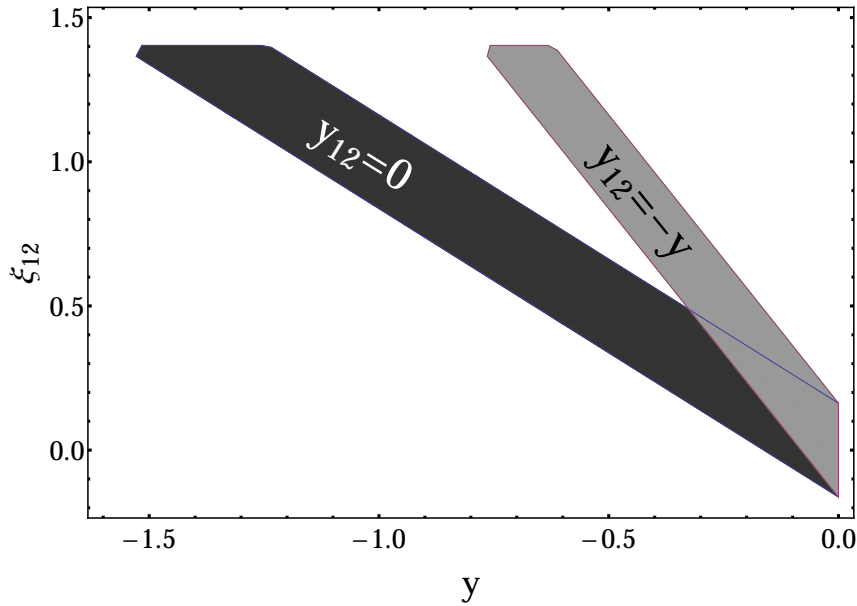


Figure 2: The allowed values of  $y$ - $\xi_{12}$ , in order to satisfy the earth constraints, for  $\Lambda = 1$  TeV and  $M_D = 300$  GeV.

A numerical example of the combination of the ‘‘Earth constraints’’ is shown in Fig. 2. Generally, combining all the aforementioned bounds, results to a lower allowed value for the doublet mass parameter ( $M_D$ ) at  $\sim 90$  GeV. Furthermore,  $\xi_{12}$  is restricted to (relatively) small values. Also

the allowed Yukawa couplings follow the relation  $\xi_{12} \approx -(2)y \pm 0.16$ , for  $y_{12} = 0$  ( $y_{12} = -y$ ). This relation, then, also restricts  $y$  to small values.

## 5. Cosmological and astrophysical constraints

Having examined the constraints imposed from earth-based experiments, we now can calculate the relic abundance of the lightest particle ( $\chi_1^0$ ) of this model and delineate the parameter space in which  $\Omega h^2$  is the observed one. After that, various other astrophysical constraints are going to be considered.

### The role of the dipoles

Before moving on, we should remind that the dipole operators (2.2) are essential in our study. This is because  $d_W$  acts as a regulator that minimizes the total annihilation cross-section as the desired EW WIMP mass tends to amplify it<sup>4</sup>. Thus this minimization is vital for obtaining cosmologically acceptable relic abundance for  $m_{\chi_1^0}$  at the electroweak scale.

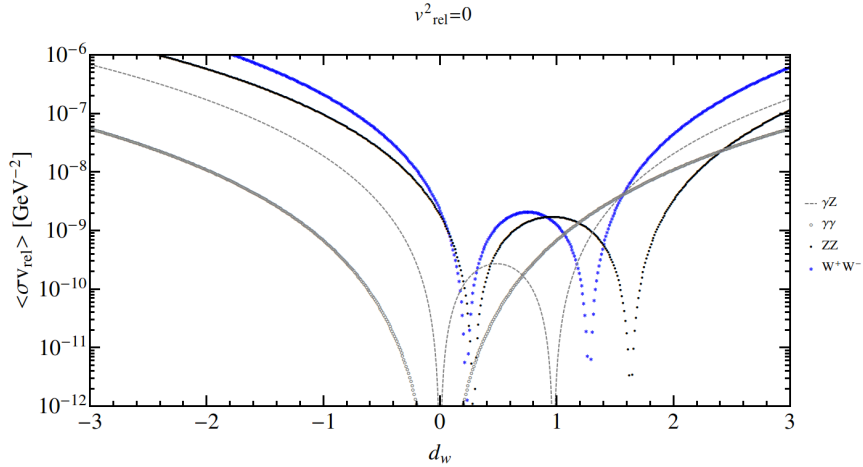


Figure 3: The dependence of the cross section for the various annihilation channels on  $d_W$  for vanishing relative velocity,  $M_D = 400\text{GeV}$ ,  $\Lambda = 1\text{TeV}$ ,  $y = -y_{12} = -\frac{\xi_{12}}{2} = -0.8$  and  $d_\gamma = 0$ .

The behaviour of the annihilation cross sections of Fig. 3 shows that there are two minima for the channels  $\chi_1^0 \chi_1^0 \rightarrow ZZ$  ( $ZZ$ -channel)  $W^+W^-$  ( $WW$ -channel) and  $\gamma Z$  ( $\gamma Z$ -channel) and one minimum for  $\gamma\gamma$  ( $\gamma\gamma$ -channel). The first minimum of the annihilations to  $ZZ$  and  $W^+W^-$  coincides with  $d_\gamma c_W \simeq d_W s_W$  ( $C_\gamma \simeq 0$ ) which gives small cross-sections for the  $\gamma\gamma$ - and  $\gamma Z$ -channels. On the other hand, the second minimum of the  $ZZ$ - and  $WW$ - channels is in a region where the annihilation to  $\gamma\gamma$  and  $\gamma Z$  blows up. Furthermore, for negative  $d_W$ , there are no minima and every cross section becomes quite large. Therefore, if the minimization of the cross section is indeed needed, we expect  $d_W$  to be bounded to non-vanishing positive values close to  $C_\gamma \simeq 0$ .

<sup>4</sup>Generally the cross section scales as  $M_D^{-2}$  at the renormalizable level.



### 5.1 Relic abundance constraints

Since the role of the dipole operators is pointed out, we can calculate the relic abundance and set further constraints on the parameter space. In Fig. 4 we show the  $d_\gamma - d_W$  plane of the parameter

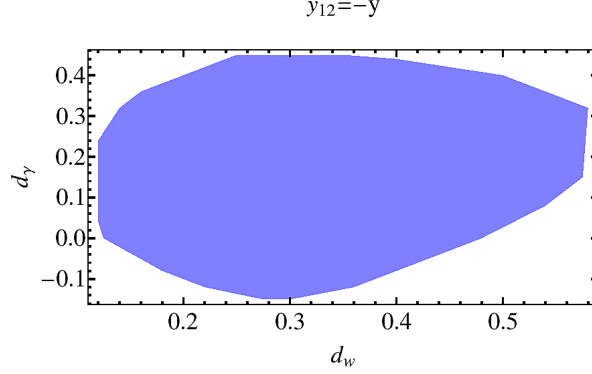


Figure 4: The plane  $d_W - d_\gamma$  of the parameter space that gives the observable relic abundance, for  $\Lambda = 1 \text{ TeV}$ ,  $y_{12} = -y$  and allowing the other parameters to vary. Similar region holds for  $y_{12} = 0$ .

space that is compatible with the observed DM relic density, varying all the other parameters, while keeping  $\Lambda = 1 \text{ TeV}$  and  $M_D \lesssim 500 \text{ GeV}$ . The parameter  $d_W$  ( $d_\gamma$ ) is bounded to be (mostly) positive in order to explain the DM relic abundance for a WIMP mass at electroweak scale, as expected from the minimization of the annihilation cross section discussed in the previous paragraph.

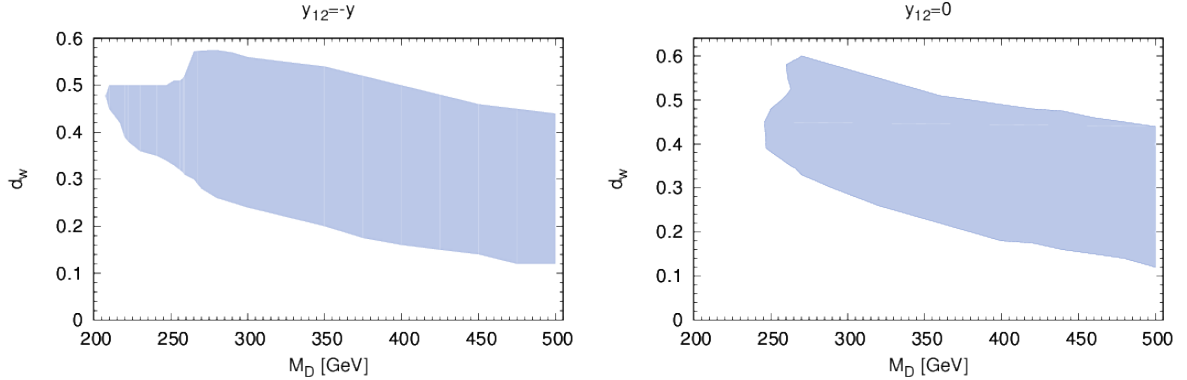


Figure 5: The acceptable values on the plane  $M_D - d_W$  for the two cases (a)  $y_{12} = -y$  and (b)  $y_{12} = 0$ , for  $\Lambda = 1 \text{ TeV}$ . Again we allow for the other parameters to vary.

From Fig. 5 we observe that  $M_D$  vastly affects the allowed values for  $d_W$  for which we obtain the observed relic abundance. This is mainly due to the dependence of the minimum of the total annihilation cross section on  $M_D$ . Additionally, as  $M_D$  increases,  $d_W$  moves to lower values, since for larger WIMP masses the minimization of the cross section is less needed (we can obtain the desired relic abundance at the renormalizable level). Also the allowed values of  $M_D - y$  are shown in Fig. 6.

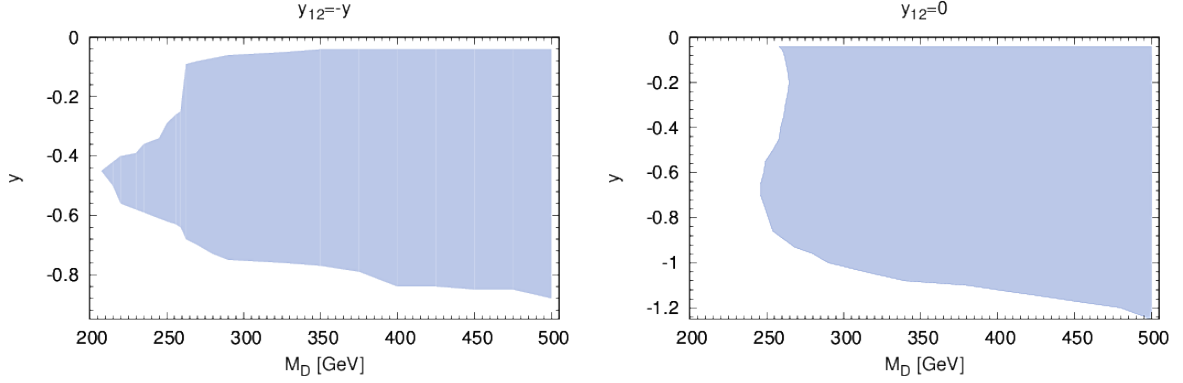


Figure 6: The acceptable values on the plane  $M_D - y$  for the two cases (a)  $y_{12} = -y$  and (b)  $y_{12} = 0$ , for  $\Lambda = 1$  TeV. The other free parameters are allowed to vary.

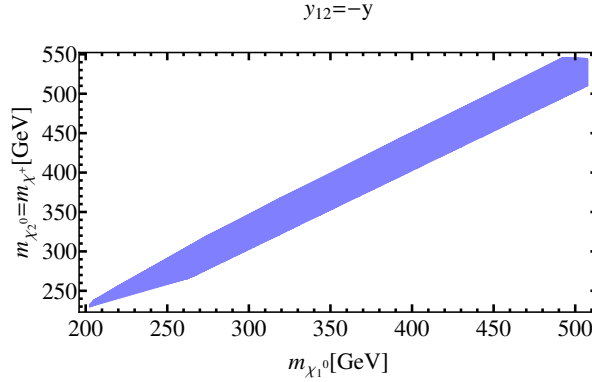


Figure 7: The allowed mass region for the case  $y_{12} = -y$ . A similar region is also allowed for  $y_{12} = 0$ .

Finally, the Yukawa couplings and the mass parameter  $M_D$  showed above, fix the masses and their differences, as expected from eq. 3.3. These masses are shown in Fig. 7 for  $y_{12} = -y$  (similar region holds also for  $y_{12} = 0$ ). We observe that the WIMP can be at the EW scale and its mass, as expected, is dominated by  $M_D$ .

## 5.2 Constraints from Gamma-ray monochromatic spectrum

In this paragraph, we calculate the cross-sections for processes that could give gamma-ray lines from the Galactic Center (GC). As input, we use the parameter space that evade all the other, previously examined, restrictions and use the results from Fermi-LAT [14] to set additional bounds to the parameters of this model.

Fro observations of gamma-ray lines from the GC show that the annihilation cross-section for  $\chi_1^0 \chi_1^0 \rightarrow \gamma\gamma$  cannot be above  $\sim 10^{-28} \text{ cm}^3 \text{ s}^{-1}$  for photon energy ( $E_\gamma = m_{\chi_1^0}$ ) at 200 GeV up to

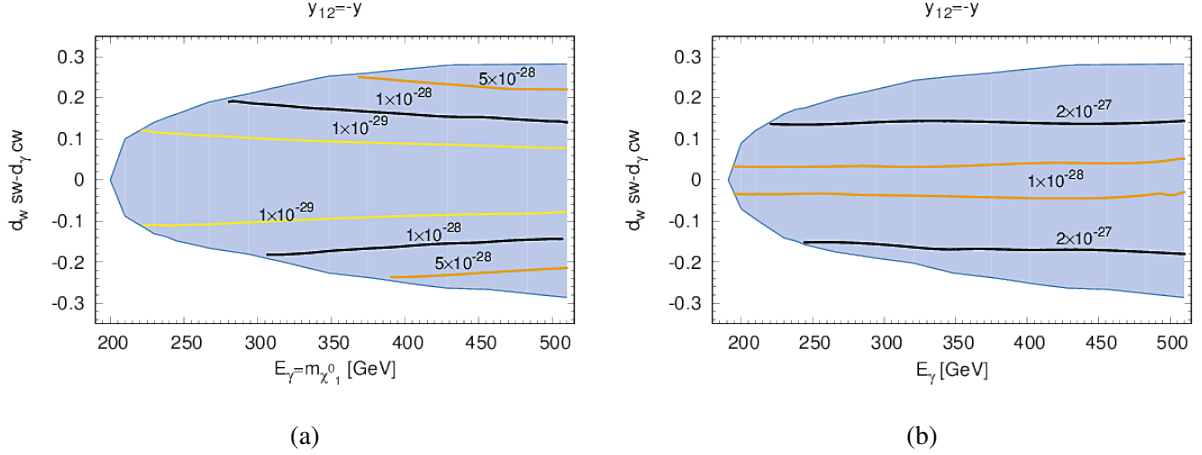


Figure 8: The allowed, region of the parameter space, in terms of the photon energy and the coupling  $d_W s_W - d_\gamma c_W$ . The contours show the values of the cross-section of the channels  $\chi_1^0 \chi_1^0 \rightarrow \gamma\gamma$  (a) and  $\gamma Z$  (b) in  $\text{cm}^3 \text{s}^{-1}$  for  $y_{12} = -y$ . Again  $y_{12} = 0$  results in an almost identical plot.

$\sim 5 \times 10^{-28}$  for  $E_\gamma \sim 500$  GeV. For the photon production channel  $\chi_1^0 \chi_1^0 \rightarrow \gamma Z$ , we need to rescale this bound by a factor of two. This process also results to different value for the photon energy given by  $E_\gamma = m_{\chi_1^0} (1 - m_Z^2/4m_{\chi_1^0}^2)$ .

The values of the relevant cross sections in the allowed region of the parameter space are shown in Fig. 8. Applying the bounds discussed above, the parameter space remains virtually unaffected, apart from the  $d_W - d_\gamma$  plane shown in figure 4.

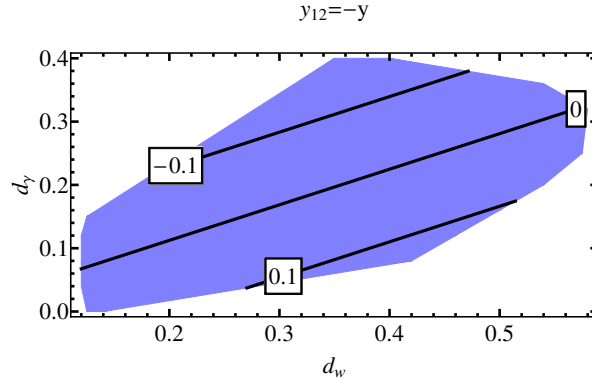


Figure 9: Allowed regions on the  $M_D - C_\gamma$  plane, consistent with “Earth” constraints, the observed relic abundance and the bounds from gamma-ray monochromatic spectrum. Almost identical regions are allowed for  $y_{12} = 0$ . The contour lines show the values of the  $\chi_1^0 \chi_2^0$ -photon coupling  $C_\gamma$ .

The values of  $d_W - d_\gamma$  which respect the bounds discussed here are shown in Fig. 9 along with  $C_\gamma$  (contours). We observe that the allowed values of  $C_\gamma$  are concentrated around zero, which forces  $d_W$  and  $d_\gamma$  to have the same sign. Thus the latter is restricted to positive values, while accepted range of  $d_W$  remains as in Fig. 4.

## 6. LHC searches

Having found the viable area in the parameter space, in which the observed DM relic abundance is obtained while avoiding all the other experimental and observational constraints, we move on to discuss possible observational effects at the LHC.

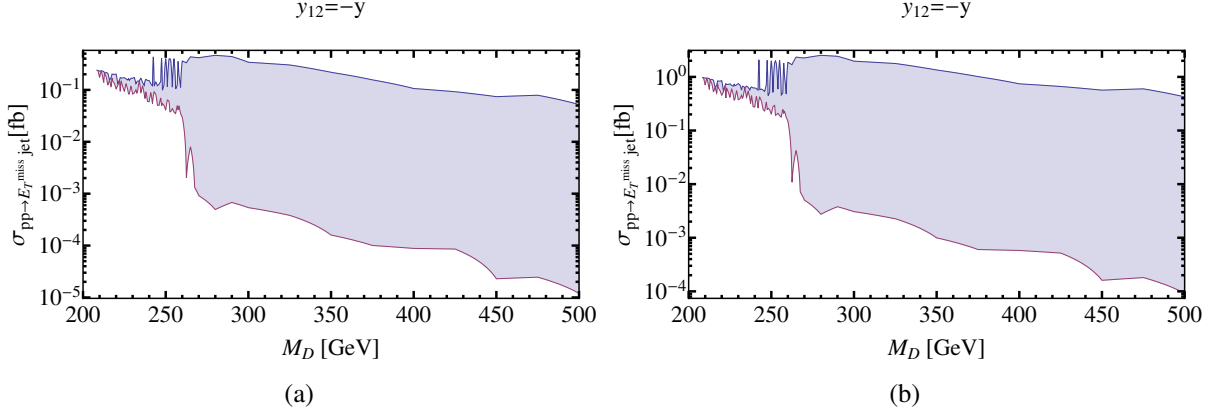


Figure 10: The cross-section for the mono-jet channel with (a)  $\sqrt{\hat{s}} = 8\text{TeV}$  and (b)  $\sqrt{\hat{s}} = 13\text{TeV}$ . The areas are obtained from randomly selected values from the ones satisfying all the constraints discussed in the previous sections.

In Fig. 10 we show the mono-jet channel cross section, which seems to be the most promising one, at least for this model. The current bound [15] on  $pp \rightarrow \chi_1^0 (\chi_2^0 \rightarrow \chi_1^0 + \nu\bar{\nu}) + jet$  at center of mass energy  $\hat{s} = 8\text{TeV}$  is  $\sigma_{\dot{E}_T+jet} \lesssim 6.1\text{fb}$ . It is apparent that this bound is easily evaded in the allowed parameter space. For LHC (RunII) at  $\sqrt{\hat{s}} = 13\text{TeV}$ , the mono-jet channel can provide us with a relatively large number of events. From Fig. 10b, we observe that the production of a jet accompanied with missing  $E_T$ , can reach cross sections up to  $\sim 2.5\text{fb}$ . Therefore the number of events that can, in principle, be observed is around 250 (750) for LHC expected luminosity reach of 100 (300)  $\text{fb}^{-1}$ .

## 7. Conclusions

We have extended the SM particle spectrum by a fermionic pair of doublets,  $D_{1,2}$ , with opposite hypercharges. In addition, we have assumed a discrete  $Z_2$ -symmetry that distinguishes this Dark Sector from the SM fields. At the renormalizable level there are a neutral, and a charged Dirac, fermion. After EW symmetry breaking, due the presence of  $d = 5$  operators, the neutral Dirac fermion splits to two Majorana states. The lightest of them ( $\chi_1^0$ ), which is the WIMP candidate and a heavier neutral state,  $\chi_2^0$ . Moreover, the  $d = 5$  operators include magnetic dipole operators which are, in principle, generated by a UV-complete model, at the TeV scale. The question we ask here is whether the WIMP, with a mass around the EW scale, is compatible to the various experimental and observational data.

In order to reduce fine tuning and further simplify the parameter space, in section 2, we adopted two scenarios based on a charge conjugation symmetric limit. Then, in section 3 we showed the mass spectrum of the physical states.

In section 4, we performed an analysis based a) on scattering WIMP-nucleus scattering experiments, b) LEP searches for heavy charged fermions, as well as c) on LHC searches for the decay  $h \rightarrow \gamma\gamma$ . We found the collective bounds showed in Fig. 2.

In section 5 we calculated  $\Omega h^2$  for our WIMP candidate. In the presence of non-vanishing  $d = 5$  dipole interactions, the WIMP annihilation cross sections acquire minima, which allow for the WIMP mass to be as low as 200 GeV. Following this we also considered constraints based of monochromatic gamma-ray spectrum observations from the Galactic Center. These set the final restrictions on the parameter space, which confined the photon dipole coupling ( $C_\gamma$ ) to be  $\sim \pm 0.1$ .

Since our main goal was to be able to produce a WIMP at the electroweak scale, in order to be accessible at the LHC, in section 6 we estimated the cross section for producing  $\chi_1^0$  in association with a jet (monojet) with center of mass energy  $\sqrt{\hat{s}} = 8, 13$  TeV. Although current bounds are weak, we found that the monojet channel, can produce few hundred of events at  $\sqrt{\hat{s}} = 13$  TeV and with  $m_{\chi_1^0} \simeq 200 - 350$  GeV (see Fig. 10).

## References

- [1] **Planck** Collaboration, P. A. R. Ade et al., *Planck 2015 results. XIII. Cosmological parameters*, *Astron. Astrophys.* **594** (2016) A13, [[arXiv:1502.01589](#)].
- [2] D. Hooper, *Particle Dark Matter*, in *Proceedings of Theoretical Advanced Study Institute in Elementary Particle Physics on The dawn of the LHC era (TASI 2008): Boulder, USA, June 2-27, 2008*, pp. 709–764, 2010. [[arXiv:0901.4090](#)].
- [3] A. Dedes, D. Karamitros, and V. C. Spanos, *Effective Theory for Electroweak Doublet Dark Matter*, *Phys. Rev.* **D94** (2016), no. 9 095008, [[arXiv:1607.05040](#)].
- [4] L. Roszkowski, *Light neutralino as dark matter*, *Phys. Lett.* **B262** (1991) 59–67.
- [5] A. Dedes and D. Karamitros, *Doublet-Triplet Fermionic Dark Matter*, *Phys. Rev.* **D89** (2014), no. 11 115002, [[arXiv:1403.7744](#)].
- [6] N. Nagata, K. A. Olive, and J. Zheng, *Weakly-Interacting Massive Particles in Non-supersymmetric SO(10) Grand Unified Models*, *JHEP* **10** (2015) 193, [[arXiv:1509.00809](#)].
- [7] C. Garcia-Cely and J. Heeck, *Phenomenology of left-right symmetric dark matter*, [[arXiv:1512.03332](#)]. [[JCAP1603,021\(2016\)](#)].
- [8] P. Sikivie, L. Susskind, M. B. Voloshin, and V. I. Zakharov, *Isospin Breaking in Technicolor Models*, *Nucl. Phys.* **B173** (1980) 189–207.
- [9] **LUX** Collaboration, D. S. Akerib et al., *Improved Limits on Scattering of Weakly Interacting Massive Particles from Reanalysis of 2013 LUX Data*, *Phys. Rev. Lett.* **116** (2016), no. 16 161301, [[arXiv:1512.03506](#)].
- [10] **LUX** Collaboration, D. S. Akerib et al., *First results from the LUX dark matter experiment at the Sanford Underground Research Facility*, *Phys. Rev. Lett.* **112** (2014) 091303, [[arXiv:1310.8214](#)].
- [11] **L3** Collaboration, P. Achard et al., *Search for heavy neutral and charged leptons in  $e^+e^-$  annihilation at LEP*, *Phys. Lett.* **B517** (2001) 75–85, [[hep-ex/0107015](#)].
- [12] A. Djouadi, *The Anatomy of electro-weak symmetry breaking. I: The Higgs boson in the standard model*, *Phys.Rept.* **457** (2008) 1–216, [[hep-ph/0503172](#)].

- 
- [13] **ATLAS, CMS** Collaboration, G. Aad et al., *Combined Measurement of the Higgs Boson Mass in pp Collisions at  $\sqrt{s} = 7$  and 8 TeV with the ATLAS and CMS Experiments*, *Phys. Rev. Lett.* **114** (2015) 191803, [[arXiv:1503.07589](#)].
- [14] **Fermi-LAT** Collaboration, M. Ackermann et al., *Updated search for spectral lines from Galactic dark matter interactions with pass 8 data from the Fermi Large Area Telescope*, *Phys. Rev.* **D91** (2015), no. 12 122002, [[arXiv:1506.00013](#)].
- [15] **CMS** Collaboration, V. Khachatryan et al., *Search for dark matter, extra dimensions, and unparticles in monojet events in proton–proton collisions at  $\sqrt{s} = 8$  TeV*, *Eur. Phys. J.* **C75** (2015), no. 5 235, [[arXiv:1408.3583](#)].